Far Infrared Studies of Bismuth

W. S. BOYLE AND A. D. BRAILSFORD*
Bell Telephone Laboratories, Murray Hill, New Jersey
(Received August 1, 1960)

The zero-field and magneto-optic studies of bismuth reported here cover a range of frequencies where the plasma effects are large and rapidly changing. It is found that the data lend themselves to an interpretation in terms of classical magneto-plasma theory when anisotropy is taken into account. The contribution of the free carriers to the optical properties can be isolated from the interband transitions and hence the static value of the dielectric constant, ϵ_0, the number of free electrons per cc, n, and the effective-mass parameters for the electron band can be determined when used in conjunction with the results of cyclotron resonance studies.

I. INTRODUCTION

IN two previous communications we have reported briefly some observations on the infrared magneto-optic properties of bismuth single crystals.[1,2] In this paper we shall present new data which is more detailed and a discussion which is an amplification of some of the points discussed earlier.

At this time, a number of independent experiments have been used to investigate the band structure of bismuth.[3–9] It is generally agreed that the charge carriers form highly anisotropic groups in momentum space having small effective masses as the result of the close approach of two bands. We shall review some of the experimental results in detail later (Sec. 5) but at present we merely mention that the number of free carriers is of the order of 5×10^{17} cm^{-3} and the effective mass parameters range down to 0.008 m_0, where m_0 is the free electron mass. The small carrier concentration places the plasma frequencies in the infrared, allows transmission experiments to be performed on bulk samples, and the small effective mass leads to large magneto-optic effects at infrared frequencies with modest magnetic fields.

The infrared data presented here does not enable one to find all the parameters necessary for a complete determination of the band structure. However, this is a feature which is common to all the different experiments used so far and so does not detract from the general methods. What it does furnish is the most direct determination of two effective mass parameters for the electron band, the static dielectric constant of the crystal, and the number of free charge carriers. When used in conjunction with the results of cyclotron resonance, the present data allow a generally consistent band model to be constructed.

II. THEORY

The problem of relating the experimental results of reflection or transmission of the infrared signal from the sample to the electron band structure can be separated into two phases. First the propagation constants for electromagnetic radiation of appropriate polarization modes is deduced from an assumed model of the band structure, and then the solution is completed by applying the boundary conditions for the fields at the sample interfaces. This last point warrants some amplification because it should be emphasized that the singularities in the optical properties at or near the plasma frequencies are not a result of the excitation of longitudinal plasma oscillations. In our experiments and also in all *optical* experiments known to us, the geometry is such that the radiation field does not couple to the longitudinal plasma modes. In the optical experiments one is dealing essentially with a plane wave at normal incidence on an infinite medium, edge effects can be neglected and $\nabla\mathbf{E}=0$ throughout. The anisotropies complicate the calculations somewhat and may lead to polarization conversion at the interfaces. Furthermore, the addition of a magnetic field can introduce nondiagonal components of the conductivity tensor which for certain orientations can lead to an induced current normal to the surface of the sample. This is one situation in which $\nabla\mathbf{E}\neq0$ and the space charge fields which build up on the surface can in this case couple to the plasma modes. We believe this to be a fruitful field of investigation but will not report any experimental results for this geometry in this paper.

In analyzing the experimental data we shall use classical magneto-ionic theory. The response of the charge carriers is described within the framework of effective mass theory, using the band model for the electrons originally proposed by Shoenberg.[3] In the region of magnetic fields and frequencies used in our experiments the holes make only a small contribution to the dielectric constant and are neglected in the

* Now at Scientific Laboratory, Ford Motor Company, Dearborn, Michigan.

[1] W. S. Boyle, A. D. Brailsford, and J. K. Galt, Phys. Rev. **109**, 1396 (1958).
[2] W. S. Boyle and K. F. Rodgers, Phys. Rev. Letters **2**, 338 (1959).
[3] D. Shoenberg, Proc. Roy. Soc. (London) **170**, 341 (1939).
[4] J. S. Dhillon and D. Shoenberg, Trans. Roy. Soc. (London) **248**, 1 (1955).
[5] J. E. Aubrey and R. G. Chambers, J. Phys. Chem. Solids **3**, 128 (1957).
[6] J. K. Galt, W. A. Yager, F. R. Merritt, B. B. Cetlin, and A. D. Brailsford, Phys. Rev. **114**, 1396 (1959).
[7] D. H. Reneker, Phys. Rev. **115**, 303 (1959).
[8] G. E. Smith, Phys. Rev. **115**, 1561 (1959).
[9] R. J. Keyes, A. Zwerdling, S. Foner, H. H. Kolm, and B. Lax, Phys. Rev.**104**, 1805 (1956).

subsequent analysis. The real part of the dielectric constant arising from interband mixing, ϵ_0, is treated as independent of frequency, an assumption which we show later to be consistent with the data.

The solution of the electromagnetic problem for the model outlined above has already been given in detail.[6] The details which are relevant to the present discussion are briefly outlined in Appendix I. We shall be interested in reflection from bismuth when radiation is incident normal to the surface of the sample and parallel to either the trigonal axis or a binary axis. Under these conditions, in the absence of a magnetic field and neglecting relaxation effects, the propagation constants are simply related to the band structure parameters. Labelling the principal crystallographic axes as follows: binary axis, 1; bisectrix 2; trigonal axis 3; and denoting $\mathbf{E}$ the vector amplitude of the electric field of frequency ω and wave vector $\mathbf{k}$; for the geometry indicated, the following relations are derived in Appendix I:

(1) $\mathbf{k}\|1$:

(a) $\mathbf{E}\|3$, $\eta_{13}^2=\epsilon_0-4\pi ne^2\alpha_{33}/m_0\omega^2$, (1a)

(b) $\mathbf{E}\|2$, $\eta_{12}^2=\epsilon_0-4\pi ne^2(\alpha_1+\alpha_2)/2m_0\omega^2$, (1b)

(2) $\mathbf{k}\|3$: $\eta_3^2=\eta_{12}^2$ independent of polarization. (2)

Here n is the number of electrons per cc; α_1, α_2 are two components of the reciprocal mass tensor, expressed in units of m_0^{-1} (we use Shoenberg's[3] notation for the α's) and $\eta^2=(ck/\omega)^2$.

From the relations (1) and (2) the frequencies at which minimum reflection occurs can be deduced by setting the appropriate $\eta=1$. In our previous paper we called this singularity a dielectric anomaly. At a slightly smaller frequency η becomes pure imaginary and within our approximation of effectively infinite relaxation time the sample exhibits perfect reflection and this appears also as a low-frequency cutoff in the transmission of the sample. It will be noted from Eqs. (1) that with radiation propagated along a binary axis and linearly polarized parallel or perpendicular to the trigonal axis, the corresponding cutoff frequencies $\omega_{\|}$ or $\omega_\perp$, are related by

$$(\omega_{\|}/\omega_\perp)^2=2\alpha_3/(\alpha_1+\alpha_2). \tag{3}$$

The application of a magnetic field influences the kinematics of the charge carriers and, of course, thereby changes the optical properties of the medium. This is manifest in the motion of the dielectric anomalies with applied magnetic field and frequency. In general, with the band model we are using the functional dependence of the positions of the anomalies upon magnetic field and frequency is quite complicated. Moreover the plane polarized electromagnetic modes we have used cease to be independent and a certain amount of polarization conversion occurs in reflection from the sample. However, in two limiting cases, namely small magnetic fields or large magnetic fields and high frequencies, it is possible to obtain simple relations between experimentally determined quantities and the band parameters without too much tedious algebra. We have treated the latter case in our previous publication[1] and so will not discuss it further here. We now turn to the behavior of the optical properties at small magnetic fields and at frequencies near the appropriate plasma frequency.

In order to avoid inessential details, consider first of all the motion of a group of charge carriers of isotropic effective mass subject to circularly polarized radiation of frequency ω. Neglecting relaxation effects the conductivity of the group is[10]

$$\sigma=ne^2/im(\omega-\omega_c), \tag{4}$$

where $\omega_c=eB/mc$ is the cyclotron resonance frequency, B the magnetic field strength, and m the effective mass. It is evident from (4) that at magnetic fields such that $\omega_c\ll\omega$ the conductivity has approximately its zero-field value. Moreover, if there are several groups of carriers of differing effective mass, at low magnetic fields the variation of the conductivity, and hence the optical properties, is essentially determined by the group of carriers with the smallest effective mass. This conclusion is not affected by extending the analysis to include the effects of linear polarization or anisotropic conductivity and is very helpful in obtaining further information from infrared experiments.

Returning to bismuth, the foregoing remarks are most appropriate when the magnetic field is normal to the surface of the sample and parallel to a binary axis. With this geometry, the results of cyclotron resonance and de Haas-van Alphen effect measurements shows that there is a group of electrons with a cyclotron mass at least ten times smaller than that of any other group. Accordingly we have calculated the positions of the dielectric anomalies for this geometry taking into account the field dependence of the current arising from the low mass group only. As indicated in Appendix I, we find that the locus of each anomaly is

$$\frac{\omega^2-\omega_{\|}^2}{\omega_{\|}^2}\cong\frac{\alpha_1\alpha_3}{2}\left(\frac{\omega_{\|}^2}{\omega_{\|}^2-\omega_\perp^2}\right)\frac{\omega_c^2}{\omega^2}, \tag{5}$$

and

$$\frac{\omega^2-\omega_\perp^2}{\omega^2}\cong-\frac{\alpha_1\alpha_3}{4}\left(\frac{3\omega_\perp^2-\omega_{\|}^2}{\omega_{\|}^2-\omega_\perp^2}\right)\frac{\omega_c^2}{\omega^2}. \tag{6}$$

Here $\omega_c=eB/m_0c$. At the small fields we are considering the anisotropy causes only a slight amount of polarization conversion and this does not affect the positions of singularities in the reflection coefficient as determined by these equations. It will be noted from (5) and (6) that when $1<\omega_{\|}/\omega_\perp<\sqrt{3}$ [see Sec. IV(A)] the difference between the two cutoff frequencies increases with

[10] P. W. Anderson, Phys. Rev. **100**, 749 (1955).

increasing magnetic field strength. Also, it is possible by either of these relations to obtain a value of $\alpha_1\alpha_3$ from the experimental data. Fortuitously, this parameter may also be obtained directly from a cyclotron mass with the field along a bisectrix direction. In view of the approximations made in this part of the analysis the latter value may be more preferable but in any case the value we obtain from our data may be used in comparison to check our interpretation of the transmission cutoffs as dielectric anomalies and our neglect of the hole band. Moreover, since all other experiments indicate that $\alpha_2 \ll \alpha_1$, ($\alpha_2 \sim 0.01\alpha_1$), we may, using (5) and (6) and (3) obtain α_1 and α_3 at once.

In Sec. IV(B) we shall have occasion to refer to the theory of cyclotron resonance. This is adequately covered in the literature and we shall merely indicate the physical basis of the results. Referring to Eqs. (A2) and (4), the propagation constant for an isotropic group of carriers is

$$\eta = [\epsilon_0 - 4\pi ne^2/m\omega(\omega-\omega_c)]^{\frac{1}{2}}. \quad (7)$$

At frequencies well below the plasma frequency, ϵ_0 is negligible compared with the contribution of the charge carriers. Since the power transmitted into the sample is proportional to η^{-1} and $\eta^{-1}\alpha[\omega(\omega_c-\omega)]^{\frac{1}{2}}$, the reflection falls off sharply with increasing field at the cyclotron resonance field, $B_c=\omega mc/e$, the decrease in reflection being proportional to $(B-B_c)^{\frac{1}{2}}$. Again, sufficiently close to the resonance of a particular group of carriers, these conclusions are not affected by the presence of other carriers or the anisotropy of the band structure (providing of course that effective mass theory is adequate).

III. EXPERIMENTAL DETAILS

The optical system has been described in detail elsewhere[11] with the minor modifications noted below. Briefly it consists of a Perkin Elmer Model 112 spectrometer modified in some cases by replacing the prism and mirror with suitable diffraction gratings. With a CsBr prism and two gratings blazed at 45 and 120 microns the spectrum from 15 to 130 microns was spanned continuously. Suitable filters, scattering plates, residual ray mirrors and choppers kept stray radiation below 5% over the whole spectrum. All experiments were performed at 2°K. For the transmission measurements a double detector system was used, with one carbon bolometer mounted behind the sample and a second detector in the cryostat was located to intercept a small fraction of the beam to provide a normalizing signal. In the case of the reflection experiments a beam was multiply reflected at nearly normal incidence from the sample surface before reaching the detector. The magnetic field was always applied normal to the sample surface.

In some cases the samples were obtained by cutting with an acid string saw, small sections from oriented boules supplied by J. Wernick. These were then polished with a final treatment in which at least 0.002 in. was etched from the surface. Other samples in particular those used in transmission, where obtained by melting sheets of the metal held between flat glass plates. A thin layer of rock salt was evaporated onto the glass surfaces to prevent adherence of the bismuth films. Either by slow cooling or by passing a molten zone through the film large single crystal areas could be obtained. No attempt was made to seed the growth and fortunately well oriented crystals with either a threefold or binary axis normal to the plane occurred during the normal growth of the crystals. The films obtained in this way were particularly useful in determining the refractive index from the well-defined interference fringes.

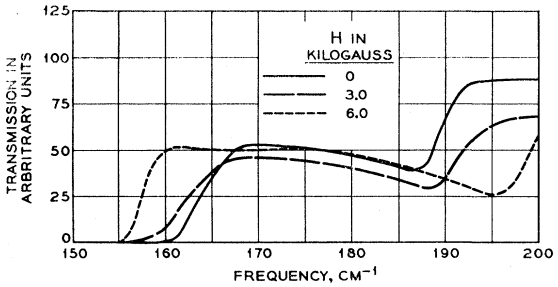

FIG. 1. Transmission spectrum of Bi No. 2 for propagation along a binary axis.

Designation	Thickness, microns	Orientation	Preparation
Bi No. 1	14.7	Trigonal	Grown
Bi No. 2	24.2	Binary	Cut, etch
Bi No. 3	Bulk	Binary	Cut, etch
Bi No. 4	43.2	Binary	Grown

IV. EXPERIMENTAL RESULTS

A. Zero-Field Data

At long wavelengths, in the region of 60 microns, we have reported two singularities in the reflection coefficient, at normal incidence, for a crystal face normal to a binary axis and a single minimum for the trigonal orientation.[1] These we ascribed to dielectric anomalies.

The data obtained from transmission experiments are shown in Fig. 1. The solid curve is for zero magnetic field and propagation along a binary axis; as in the case of the reflection data, two low-frequency cutoffs are observed. The other two dashed curves in Fig. 1 show the motion of the cutoffs with magnetic field, we note in particular that they move apart with increasing magnetic field. We note also that the low-frequency cutoff, at zero field, for propagation along a binary axis agrees quite well with the corresponding frequency, 156 cm^{-1}, in a trigonal sample, as shown in Fig. 2. All these facts confirm the theoretical analysis of Sec. II.

In Table I we give the frequencies obtained from plots such as Fig. 1 for two different samples and

[11] W. S. Boyle and K. F. Rodgers, J. Opt. Soc. Am. 49, 66 (1959).

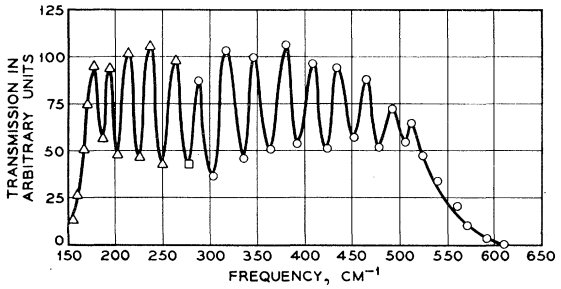

FIG. 2. Interference fringes obtained in Bi No. 1. The regions covered by the points Δ and 0 are from grating and prism measurements, respectively.

compare these with the minima in the reflection coefficient described in reference 1. From this data we obtain the mean value,

$$2\alpha_3/(\alpha_1+\alpha_2)=1.37.$$

We have obtained well-defined interference in crystals of both binary and trigonal symmetry. The data for the trigonal case is shown in Fig. 2 and similar results were obtained for the binary sample. In the binary case however it was not possible to isolate the interference from the two polarizations and we have not been able to extract any reliable results.

Because of the rapid variation of the refractive index with frequency it is not possible to determine the order of the interference fringes from the usual plot of the fringe number versus frequency. We were fortunate however in being able to obtain samples sufficiently thin so that the last fringe before the cutoff was a number of order one. The proper and unambiguous order could then be obtained by choosing a value which gave an extrapolated value of the refractive index which was reasonably consistent with the reflection or transmission determination of the points at which the refractive index was zero or one. Sample thickness was determined by weighing and the refractive index calculated from the expression $N\lambda_n=2\mu d$ for the wavelengths of the maxima. Here d is the thickness of the sample and μ the refractive index. The frequency dependence for μ^2 is shown in Fig. 3. Since $\eta=\mu$, we see from Eqs. (1b) and (2) that μ^2 should satisfy a relation of the type

$$\mu^2=\epsilon_0-\omega_0^2/\omega^2, \tag{7}$$

where $\omega_0^2=4\pi ne^2(\alpha_1+\alpha_2)/2m_0$, and ϵ_0 is a constant. For frequencies ≤ 400 cm^{-1}, Eq. (7) describes the data extremely well with $\epsilon_0=99.6$ and $\omega_0=162.2$ cm^{-1}. Alternatively, we may assume this value of ω_0 and Eq. (7) to determine ϵ_0 as a function of frequency. The derived value of ϵ_0 at higher frequencies is shown in Fig. 3, and is seen to be essentially constant over the whole range of measurements apart from a slight increase at the highest frequencies.

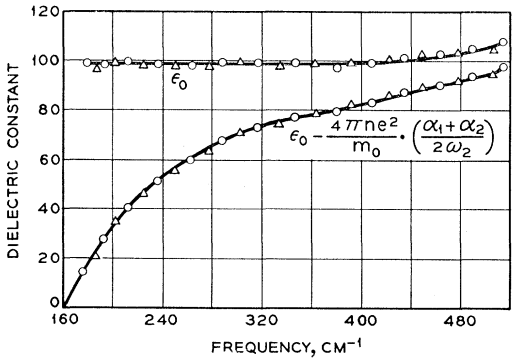

FIG. 3. The lower curve is the value of the dielectric constant derived from Fig. 2 and fitted by the expression given below the curve. A two point fit was made at 175 and 240 cm^{-1} and then the remainder of the curve used to derive the value of ϵ_0 plotted in the upper part of the diagram.

In going to higher frequencies there is a strong absorption which sets in strongly in the neighborhood of 20 microns. The position of this edge is independent of sample orientation and is independent of the polarization of the radiation. We have not made absolute measurements on the transmission coefficient with any precision, but the large increase in the absorption coefficient that we see in Fig. 2 is typical of all samples that we have studied.

TABLE I. Cutoff frequencies for propagation along a binary axis.

Sample	$\omega_\perp$ (cm^{-1})	ω_{II} (cm^{-1})	$2\alpha_3/\alpha_1+\alpha_2$
Transmission Bi No. 2	161	188	1.36
Transmission Bi No. 4	159.5	186	1.36
Reflection Bi No. 3	158	186	1.38

B. Magneto-Optic Data

In discussing Fig. 1 we have already mentioned the motion of the cutoff frequencies with magnetic field. Figure 4 shows in more detail the variation of the high frequency dielectric anomaly when the field and propagation vector are along a binary axis. According to Eq. (5), a plot of $(\omega/\omega_{II})^2$ vs $(\omega_c/\omega)^2$ should be linear. The reflection data is presented in this form in Fig. 5, where we have used the minimum in the reflection to determine the frequency ω. There is clearly a deviation from the linear relationship at the largest field where the approximations we made in deriving (5) begin to break down. From the slope at the smallest fields we find

$$1/2\{\alpha_1\alpha_3/[1-(\omega_\perp/\omega_{II})^2]\}=1.5\times10^4,$$

and using our previous result for $(\omega_{II}/\omega_\perp)^2=1.37$, we calculate $\alpha_1\alpha_3=8.1\times10^3$. As mentioned earlier, we may use this value of $\alpha_1\alpha_3$ to calculate a cyclotron mass for the field along a bisectrix. This is

$$m_{2a}{}^*=\frac{m_0}{(\alpha_1\alpha_3)^{\frac{1}{2}}}=0.011m_0,$$

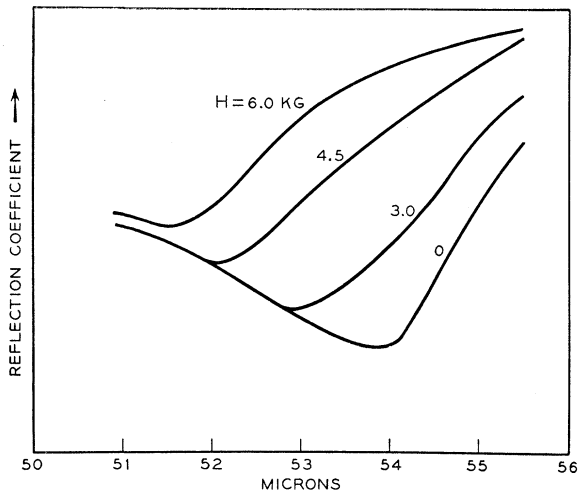

FIG. 4. The motion of the higher frequency dielectric anomaly with magnetic field along a binary axis as observed in reflection from a surface normal to the binary axis.

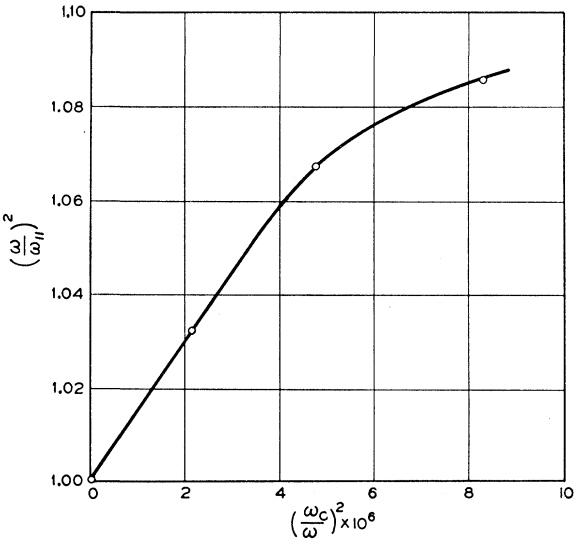

FIG. 5. The frequency of the dielectric anomaly, ω, from Fig. 4 plotted as a dimensionless ratio $(\omega/\omega_{11})^2$ versus a reduced magnetic field ω_c/ω, as suggested by Eq. (5).

whereas by direct measurements from cyclotron resonance[6] the value obtained is $m_{2b}{}^*=0.009m_0$. The agreement is quite good and adds support to our interpretation of the data.

Finally we report one direct observation of cyclotron resonance at infrared frequencies. Figure 6 shows data taken at 87 microns with the field and direction of propagation along a binary axis. The curve has the form expected apart from the slow decrease in reflection prior to the sharp break. This is doubtless due to finite relaxation time effects which we neglected in our earlier discussion. We extract a cyclotron resonance field by extrapolation as shown in the figure to obtain $B_c = 12\,800$ gauss. At 87 microns this sets the effective cyclotron mass at $m_{1b}{}^*=1.04\times10^{-2}\ m_0$. This is in excellent agreement with other reported values for this orientation.[5,6]

This completes the description and analysis of the infrared data.

V. DISCUSSION

The infrared data, when used in conjunction with the results of cyclotron resonance (with the magnetic field both perpendicular[6] and parallel[5] to the sample surface) give a consistent picture of the band structure of bismuth.

TABLE II. Cyclotron masses for electrons.[a]

$m_{1a}=m_0/[(\alpha_2\alpha_3-\alpha_4^2)]^{\frac{1}{2}}$	0.11 m_0[b] or 0.13 m_0[c]
$m_{1b}=2m_{1a}m_{2a}/[(3m_{1a}{}^2+m_{2a}{}^2)]^{\frac{1}{2}}$	0.01 m_0[b,c,d]
$m_{2a}=m_0/[(\alpha_1\alpha_3)]^{\frac{1}{2}}$	0.009 m_0[c]
$m_{2b}=2m_{1a}m_{2a}/[(m_{1a}{}^2+3m_{2a}{}^2)]^{\frac{1}{2}}$	0.018 m_0[c]
$m_3=m_0/[(\alpha_1\alpha_2)]^{\frac{1}{2}}$	0.08 m_0[c]

[a] The notation m_i denotes a cyclotron mass when the magnetic field is along axis i $(i=1,2,3)$.
[b] See reference 5.
[c] See reference 6.
[d] Present work.

In Table II we have listed the cyclotron masses for the electrons, their dependence upon the α's, and the numerical values obtained from the data. The independent determinations are in good agreement, in the one case where there is a difference (m_{1a}) we use the average value. It will be noted that there are only three independent masses and four α's, so that additional information is required. This is the source of most of the apparent discrepancy between the different published values of these parameters. However, with our independent determination of α_3/α_1, we can now obtain a set of values derived from optical properties only. These are:

$$\alpha_1=133,\quad \alpha_2=1.2,\quad \alpha_3=91,\quad \alpha_4=6.1.$$

With the above α_1 and α_3 we may then calculate the density of electrons from the value $\omega_0=162.2$ cm^{-1}, which gives $n=4.4\times10^{17}$ cm^{-3}. The Fermi energy for the electrons E_e is related to the carrier density

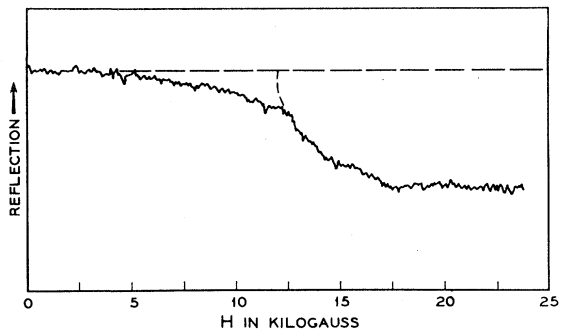

FIG. 6. The reflection in arbitrary units as a function of magnetic field for the field and incident radiation both along a binary axis.

TABLE III. Comparison of electron band parameters with those obtained from anomalous skin effect. The units of α_i/E_e are 10^3/ev.[a]

	α_1/E_e	α_2/E_e	α_3/E_e	α_4/E_e
Calculated	8.87	0.080	6.06	0.41
A.S.E. (specular)[a]	9.1	0.088	4.7	0.38
A.S.E. (diffuse)[a]	6.4	0.062	3.3	0.27

through the relation

$$n=r\frac{8\pi}{3h^3}\frac{(2m_0E_e)^{\frac{3}{2}}}{[\alpha_1(\alpha_2\alpha_3-\alpha_4^2)]^{\frac{1}{2}}},$$

where r is the number of ellipsoids in the electron band. Following Smith,[8] we assume $r=6$ and find $E_e=0.015$ ev. We now compare the values of α_i/E_e we obtain with those derived from an analysis of the anomalous skin effect (A.S.E.).[8] in Table III. The quoted error in the latter work is 20%, whereas the data in Table II is stated to be within 10%. The agreement between the different sets is therefore very good.

We may repeat the same analysis for the hole band assuming two ellipsoids of revolution about the trigonal axis. From the cyclotron masses[6]

$$M_a^*=0.068\ m_0 \quad \text{and} \quad M_b^*=0.25\ m_0,$$

with the magnetic field along and perpendicular to the trigonal axis, we find for the reciprocal mass parameters in the hole band,

$$\beta_1=14.7 \quad \text{and} \quad \beta_3=1.07.$$

Assuming that the number of holes and the number of electrons are equal we use the relations

$$n=2\frac{8\pi}{3h^3}\frac{(2m_0E_h)^{\frac{3}{2}}}{(\beta_1^2\beta_3)^{\frac{1}{2}}},$$

to determine the Fermi energy for the holes, E_h. We obtain $E_h=0.0082$ ev. We then calculate β_i/E_h and compare with the results of A.S.E. in Table IV. There is again quite good agreement well within experimental error.

We may also calculate the periods to be expected from de Haas-van Alphen type experiments (all magneto-oscillatory phenomena are included in this general category). According to the simplest form of the theory,[12] the period of oscillations, P, of the observed physical quantity is $P=\mu m_0/E_f m^*$ where μ is the double Bohr magneton, m^* the cyclotron effective mass and E_f the Fermi energy of the group of carriers. In Table V we summarize the correlation which gives the best possible agreement. The calculated values of the periods we ascribe to electrons are all slightly larger than the observed periods, with the exception of the period of 1.57×10^{-5} gauss^{-1}, listed in parentheses. However, since these deviations are less than 10% we cannot regard this as significant. Another point worthy of note is the absence of any observed period of approximately 0.6×10^{-5} gauss^{-1} with the field along a binary axis. The period of 0.3×10^{-5} gauss^{-1} with this orientation is certainly not due to electrons as can be seen from a cursory inspection of the values of the cyclotron masses and the long period, both sets being obtained by independent observers.

TABLE IV. Comparison of hole band parameters with those obtained from anomalous skin effect. Units are 10^3/ev.

	β_1/Eh	β_3/E_h
Calculated	1.8	0.13
A.S.E. (specular)[a]	1.52	0.118
A.S.E. (diffuse)[a]	1.07	0.083

[a] See reference 8.

TABLE V. Comparison of calculated and observed periods in de Haas–van Alphen effect experiments.[a]

Direction of magnetic field	Calculated period $\times10^5$, in gauss^{-1}	Observed period $\times10^5$, in gauss^{-1}
(I) Electrons		
1	0.64	
	7.7	7.1[b,c]
2	8.6	8.2[d]
	4.3	4.0[e]
3	0.96	(1.57[b,f,g])
(II) Holes		
1	0.57	0.3[e]
2	0.57	
3	2.09	(1.57[b,f,g])

[a] The first column gives the crystal axis to which the field is parallel.
[b] M. C. Steele and J. Babiskin, Phys. Rev. **98**, 359 (1955).
[c] J. Babiskin, Phys. Rev. **104**, 981 (1957).
[d] See reference 4.
[e] See reference 5.
[f] W. C. Overton, Jr., and T. A. Berlincourt, Phys. Rev. **99**, 1165 (1955).
[g] R. A. Connell and J. A. Marcus, Phys. Rev. **107**, 940 (1957).

The argument in the case of the holes is much poorer and probably beyond experimental error. A one-ellipsoid model for the hole band would bring the oscillatory experiments into better agreement with the cyclotron resonance data, giving periods of 0.36 and 1.31 compared to the observed periods of 0.3 and 1.57, all in units of 10^{-5} gauss^{-1}. However, no direct comparison is possible with the A.S.E. experiments for this case and we leave the matter as an open question.

ACKNOWLEDGMENTS

The authors wish to thank J. K. Galt, P. A. Wolff, and G. E. Smith for several valuable discussions.

APPENDIX I

The plane wave solutions, $\mathbf{E}(\mathbf{r},t)=\mathbf{E}\exp i(\omega t-\mathbf{k}\cdot\mathbf{r})$ satisfy the equations

$$[\eta^2-\epsilon_0+(4\pi i/\omega)\boldsymbol{\sigma}]\mathbf{E}=0, \qquad \text{(A1)}$$

[12] L. D. Landau, See Appendix to reference 3.

where $\eta=ck/\omega$. Suppose that the propagation is along the z axis and $\boldsymbol{\sigma}$ is of the form

$$\boldsymbol{\sigma}=\begin{vmatrix}\sigma_{xx} & \sigma_{xy} & 0\\ \sigma_{y} & \sigma_{yy} & 0\\ 0 & 0 & \sigma_{zz}\end{vmatrix}. \quad \text{(A2)}$$

Substitution of (A2) into (A1) leads to two homogeneous equations for the components E_x and E_y. The resulting secular equation has the solution

$$\eta^2=\epsilon_0-(2\pi i/\omega)\{\sigma_{xx}+\sigma_{yy} \pm[(\sigma_{xx}-\sigma_{yy})^2+4\sigma_{xy}\sigma_{yx}]^{\frac{1}{2}}\}. \quad \text{(A3)}$$

The relations used in Sec. II are special cases of (A3) as they apply to bismuth.[13] In zero magnetic field, with $\mathbf{k}\|3$,

$$\sigma_{xx}=\sigma_{yy}=\sigma_{22},$$
$$\sigma_{xy}=\sigma_{yx}=0,$$

and

$$\eta_3^2=\epsilon_0-(4\pi i/\omega)\sigma_{22}. \quad \text{(A4)}$$

Similarly, with the propagation along a binary axis $\sigma_{xy}=\sigma_{yx}=0$ and

$$\eta_{12}^2=\epsilon_0-(4\pi i/\omega)\sigma_{22}, \quad \text{(A5)}$$

$$\eta_{13}^2=\epsilon_0-(4\pi i/\omega)\sigma_{33}. \quad \text{(A6)}$$

Equations (1a), (1b), and (2) are obtained from (A6), (A5), and (A4) by substituting the expressions for σ_{ii} given in reference 13. Equations (5) and (6) were obtained by expanding the radicand in (A3) treating σ_{xy} as small.

[13] B. Lax, K. J. Button, J. J. Zeiger, and L. M. Roth, Phys. Rev. **102**, 715 (1956).

PHYSICAL REVIEW VOLUME 120, NUMBER 6 DECEMBER 15, 1960

Ferroelectric Properties of $BaLi_{2x}Al_{2-2x}F_{4x}O_{4-4x}$

T. G. Dunne and N. R. Stemple
International Business Machines Research Laboratory, Poughkeepsie, New York
(Received August 10, 1960)

Single crystals of $BaLi_{2x}Al_{2-2x}F_{4x}O_{4-4x}$, where $x=0.15$ to 0.30, have been found to be ferroelectric with a Curie temperature in the range 127–153°C and a room-temperature spontaneous polarization along the hexagonal c axis of approximately 0.1 μcoul/cm^2. The structure of these mixed crystals is unrelated to that of any previously known ferroelectric, but appears to be very similar to that of $BaAl_2O_4$.

DURING an investigation of the chemical and dielectric properties of fluoride perovskites, a new type of room-temperature ferroelectric, $BaLi_{2x}Al_{2-2x}F_{4x}O_{4-4x}$, has been discovered. Crystals have been prepared in a composition range $x=0.15$ to 0.30 and ferroelectric properties investigated.

The crystals were prepared from an equimolar mixture of LiF and BaF_2, where the BaF_2 was contaminated with 0.25 wt % Al. Crystals of $BaLi_{2x}Al_{2-2x}F_{4x}O_{4-4x}$ may also be prepared from an equimolar mixture of LiF and pure BaF_2 doped with about 0.11 wt % $AlF_3\cdot H_2O$ with respect to BaF_2. All mixtures were heated at 1300°C in a Pt crucible and cooled at a rate of 40°C per hour to well below the reported 850°C melting point of $LiBaF_3$[1] before the furnace was shut off. The resulting product consists mainly of small cubes of $LiBaF_3$ interspersed with a much smaller amount of $BaLi_{2x}Al_{2-2x}F_{4x}O_{4-4x}$ in the form of hexagonal platelets 1 to 4 mm^2 in area and about 0.1 mm thick. They were collected and analyzed for fluoride and aluminum by standard techniques. In every case the value of x calculated from aluminum analysis agreed to within 10% with that calculated from fluoride analysis. x had a value of 0.30 when Al contaminated BaF_2 was used and $x=0.20$ and 0.15 for crystals grown using pure BaF_2 doped with 0.113 wt % and 0.103 wt % Al, respectively.

The crystal structure of $BaLi_{2x}Al_{2-2x}F_{4x}O_{4-4x}$ is very similar to that found by powder pattern data for $BaAl_2O_4$.[2] The Weissenberg single-crystal data for the hexagonal unit cell of $BaLi_{0.6}Al_{1.4}F_{1.2}O_{2.8}$ gave $a=10.44$ A and $c=8.77$ A compared with $a=5.209$ A and $c=8.761$ A reported for $BaAl_2O_4$. We are attempting to grow crystals of $BaAl_2O_4$ in order to determine whether the a axis is also doubled in length in the pure compound as well as to investigate the dielectric properties.

Since the polar sixfold axis is perpendicular to the plane of the platelet, the dielectric properties of $BaLi_{2x}Al_{2-2x}F_{4x}O_{4-4x}$ were only investigated in this direction.

The 1 kc/sec^{-1} dielectric constant, ϵ, and the 60-cps spontaneous polarization, P, were determined by standard techniques.[3,4]

The experimental error for ϵ is about 100% and the

[1] A. G. Bergman and J. I. Banascheck, Ann. secteur anal. physico-chim., Inst. chim. gén. (U.S.S.R.) **23**, 201 (1953).

[2] S. Wallmark and A. Westgren, Arkiv Kemi, Mineral. Geol. **12B**, 1 (1937).

[3] S. Triebwasser, Phys. Rev. **101**, 993 (1956).

[4] C. B. Sawyer and C. H. Tower, Phys. Rev. **35**, 269 (1930).